https://doi.org/10.2352/EI.2022.34.16.AVM-109

A Review of IEEE P2020 Noise Metrics

Orit Skorka; onsemi; Santa Clara, CA, USA
Paul Romanczyk; Imatest; Boulder, CO, USA

Abstract

The IEEE P2020 Noise standard is built upon methodology that is discussed by other photography and camera standards. It includes extensions and adjustments to support operating modes and conditions that are relevant to automotive cameras. This work presents methods and procedures that are covered by the IEEE P2020 Noise standard to derive sensor-level and camera-level noise image quality factors from dark statistics, photon-transfer and signal-to-noise ratio curves, and signal falloff. Example implementations and experimental results are shown from work that was done with automotive cameras which were activated and tested under conditions that are relevant to automotive applications.

Introduction

Noise in electronic imaging systems represents the unwanted variations in pixel signal values under constant and uniform illumination. The total noise of a pixel array or sub-array includes temporal and spatial variations. Temporal noise is the fluctuations in pixel signal over time or from one frame to the other, and fixed-pattern noise (FPN) is the spatial variations in mean pixel signal across a uniformly illuminated region. Noise quantification is crucial for automotive imaging applications because it degrades image quality in viewing applications and can misguide object detection and identification blocks in machine vision systems.

Although noise is covered by several photography and camera standards, including The European Machine Vision Association (EMVA) 1288 standard, Release 4.0 Linear [1] and the International Organization for Standardization (ISO) 15739:2013 standard [2], existing standards do not fully address operating modes and conditions that are relevant to automotive cameras, such as extended temperature range, high dynamic range (HDR) scenes, raw image data in 16-bit to 32-bit format when cameras are operated in HDR modes, and wide field-of-view lenses. For that reason, the IEEE P2020 standard for automotive image quality includes a clause that is dedicated to noise [3].

Noise Image Quality Factors

This section discusses procedures to derive sensor-level image quality factors (IQFs) from dark statistics, photon-transfer curve (PTC) and signal-to-noise ratio (SNR) curves, and camera-level IQFs from signal falloff. All procedures require raw, i.e., linear, image data.

Dark Statistics

Dark noise properties of automotive cameras are important for evaluation of image quality in dim light conditions. Dark signal distribution and dark signal non-uniformity (DSNU) are used to characterize dark spatial noise, and temporal noise distribution and array temporal noise are used to characterize dark temporal noise. For data acquisition, a set of *K* frames should be captured in the dark in stable temperature conditions when the camera is activated with the same configuration file that is used by the end-user application. Mean and temporal variance can then be calculated for each pixel to produce mean signal and temporal variance images, as illustrated in Figure 1.

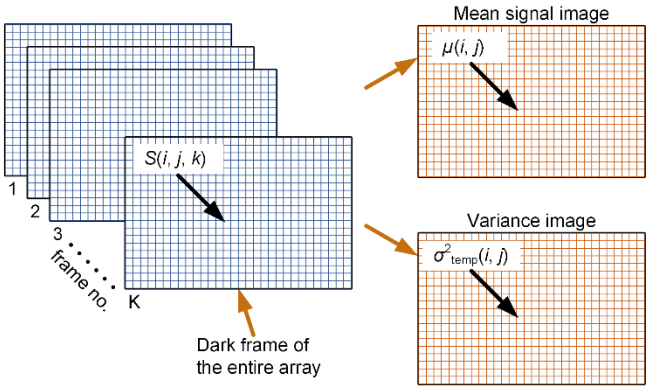

Figure 1. Dark statistics requires a set of K dark images that were captured at a stable temperature when the camera was activated with the configuration file of the end-user application. Mean and temporal variance can be calculated for each pixel to produce mean and temporal variance images.

Mean signal of the pixel in row i and column j, $\mu(i, j)$, is calculated as follows:

$$\mu(i,j) = \frac{1}{K}\sum_{k=1}^{K} S(i,j,k), \tag{1}$$

where k is frame number and S is the pixel signal in digital numbers (DNs). Mean signal of the entire array, μ, is calculated as:

$$\mu = \frac{1}{I \times J}\sum_{i=1}^{I}\sum_{j=1}^{J} \mu(i,j)\,, \tag{2}$$

where I and J are the total number of rows and columns, respectively. Fixed-pattern noise, σ_{FPN}, which is the DSNU in this case since the measurement is done in the dark, is calculated as:

$$\sigma^2_{\text{FPN}} = \frac{1}{I \times J}\sum_{i=1}^{I}\sum_{j=1}^{J} [\mu(i,j) - \mu]^2\,. \tag{3}$$

Temporal noise of the pixel in row i and column j, $\sigma_{\text{temp}}(i, j)$, is calculated as follows:

$$\sigma^2_{\text{temp}}(i,j) = \frac{1}{K-1}\sum_{k=1}^{K} [S(i,j,k) - \mu(i,j)]^2. \tag{4}$$

Array temporal noise, σ_{temp}, is calculated as:

$$\sigma^2_{\text{temp}} = \frac{1}{I \times J}\sum_{i=1}^{I}\sum_{j=1}^{J} \sigma^2_{\text{temp}}(i,j)\,. \tag{5}$$

All the expressions in (1) – (5) and in the next section are shown in a simplified format. For example, calculation and subtraction of dark signal from the total signal is not included. The IEEE P2020 Noise standard [4] includes equations in their full format with all calculation steps and calculation of row and column noise parameters. Revision 8 of the draft document was available at the time of the writing, and the reader is advised to refer to the most recent revision.

Photon-Transfer and SNR Curves

Like with dark statistics, a set of images that were captured under stable temperature conditions and with the configuration file of the end user application is needed to construct the PTC and the SNR curves of an image sensor. However, this time an image of a test target is projected on the image plane during image capture. The image of the test target includes *N* regions, where illuminance or irradiance in each region is, ideally, constant and uniform, but light level is different in each region, as illustrated in Figure 2.

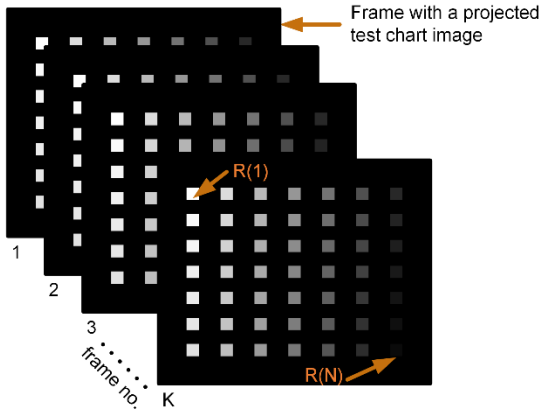

Figure 2. A set of K image frames that were captured when a test target is projected on the image plane is used to construct PTC and SNR curves. The test target includes N regions, and illumination in each region, n, in the image is constant and uniform, but different.

Equations (1)–(5) can be applied to each region. Additional expression to calculate total noise, σ_{tot}, temporal SNR, SNR_{temp}, and total SNR, SNR_{tot}, in region *n* are shown below. Analysis is based on the assumptions that (a) variations in pixel parameters are small, and (b) illumination gradients in each region are negligible.

$$\sigma_{\text{tot}}^2(n) = \sigma_{\text{temp}}^2(n) + \sigma_{\text{FPN}}^2(n); \quad (6)$$

$$\text{SNR}_{\text{temp}}(n) = \frac{\mu(n)}{\sigma_{\text{temp}}(n)}; \quad (7)$$

$$\text{SNR}_{\text{tot}}(n) = \frac{\mu(n)}{\sigma_{\text{tot}}(n)}. \quad (8)$$

Figure 3 presents simulated PTC and SNR curves of an image sensor in 3-exposure HDR mode. In this mode, the HDR response is achieved by combining frames that are captured with 3 different exposure times. The photon-transfer curve is the temporal noise versus mean signal curve; the FPN versus mean signal curve is included in the same plot. System gain (SG) is the DN to e- factor, which is the slope of the PTC curve in shot-noise limited regions [5]. The 3-exposure mode has three SG values, one for each exposure, where the one that is useful to estimate the effective number of charge carriers is the one that is closest to the origin, i.e., SG(1). Mean signal level that correlates to the effective full well, S_{EFW}, is the signal at the peak of the PTC curve.

In the SNR plot, SNR1 is the signal level at which signal equals total noise and, therefore, $SNR_{tot} = 0$ dB. Each exposure transition involves a sudden reduction in SNR [6]. The plot indicates peak and dip SNR values at the beginning and at the end of each transition region, respectively. Signal value at S_{max} is the maximum digital number that the sensor can output with the configuration file that is used for the measurement.

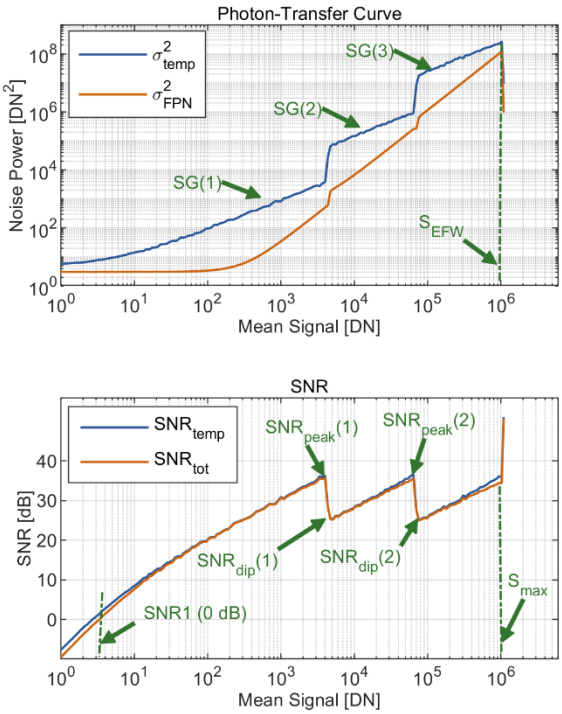

Figure 3. Simulated photon-transfer curve (top) and SNR curves (bottom) of an image sensor in 3-exposure HDR mode.

Two regions of concern in the SNR curve are SNR in dim scenes, where noise is more dominant because the photo signal is low, and the dips in the SNR curve. Figure 4 presents example images for both regions. Noise artifacts in dim light conditions are shown in an image that was captured outdoors at nighttime with an automotive camera where the main light source was the headlights of the car. Noise artifacts in the transition region are demonstrated with an image that was captured outdoors with an automotive camera that was activated in a 3-exposure HDR mode. The arrows point to regions where mean signal levels of green pixels are around the second transition of the SNR curve. Tone mapping and contrast had to be adjusted to make the artifacts more visible in the image as $SNR_{dip}(2)$ was about 25 dB, which is sufficiently high.

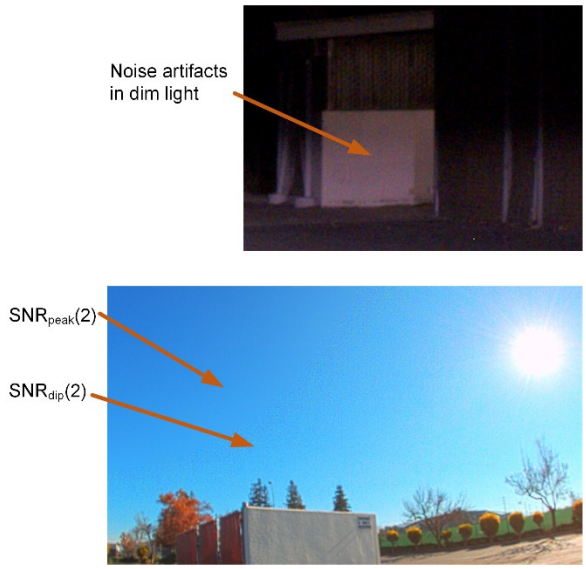

Figure 4. Noise artifacts in photos that were captured with automotive cameras. The top image was captured at nighttime in dim light conditions. The bottom image demonstrates the effect of SNR dip in the second transition region of the SNR curve of an image sensor in 3-exposure HDR mode.

Signal Falloff

Signal falloff is the low-frequency change in mean signal response across the array. It is caused by lens vignetting, angular response of camera filters, micro-lens shift, and temperature gradients in the pixel array. It is important for any application that relies on absolute radiometry, and it may impact computer vision training and detection. This metric is proposing a method to quantify the falloff by curve fitting, where the residual is used to evaluate the fit and good fits can be used to compensate for signal falloff in captured images.

Figure 5 presents 30-frame average signal falloff images of the Gr channel, i.e., green pixels in the G-R rows of the Bayer pattern. Images were captured with two automotive cameras, with 2.1 and 2.6 MP image sensors under diffused uniform illumination from a broadband source. Camera lenses were different, but both included an infrared-cut filter. The images show that signal falloff from the center to the edge of the array is steeper in camera #2.

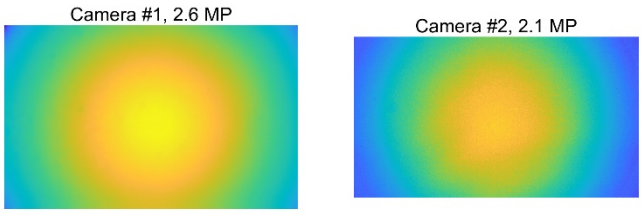

Figure 5. Signal falloff images of the Gr channel of two automotive cameras. Images were captured when the cameras were illuminated by diffused uniform light of a 6,000K source. The falloff is steeper in camera #2.

Practical Examples

This section presents experimental work that was done with automotive cameras to implement tests and procedures to extract the sensor-level and camera-level noise IQFs that were covered in the previous section.

Dark Statistics

Two sets of 44 dark images were captured with an automotive camera with an older generation 2 MP image sensor when the camera was placed in a temperature chamber and the sensor junction temperature was 40C in the first set and 80C in the second. The camera was activated with high gain and 33 ms exposure time. Figure 6 presents dark signal histogram and 1- cumulative distribution function (CDF) plots at both temperatures, which show that dark signal values and distribution increase with temperature.

DSNU, as calculated according to (3), is 9.8 DN at 40C and 74.7 DN at 80C. System gain of the image sensor at the gain that was used was 4.2 DN/e- according to the product characterization report. This value allowed to calculate DSNU in charge units, which resulted in 2.3 e- at 40C and 17.8 e- at 80C.

Figure 7 presents temporal noise variance histogram and 1-CDF plots from the same data set. Dark temporal noise is composed of dark current shot noise, which increases with temperature, and read noise. Read noise includes a thermal component, which increases with temperature, and random telegraph signal noise, which decreases with temperature. Overall, dark temporal noise increases with temperature. Temporal noise, as calculated according to (5) and after division by the SG, is 1.4 e- at 40C and 3.6 e- at 80C.

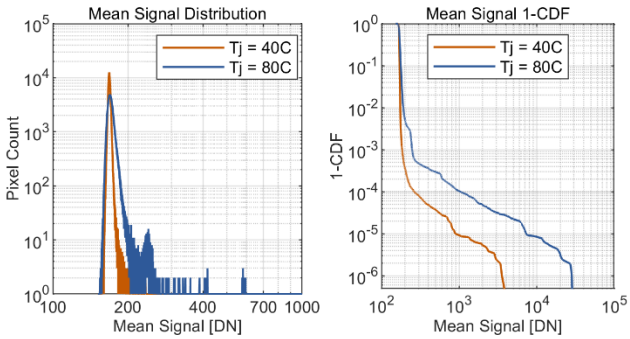

Figure 6. Mean signal histograms (left) and 1-CDF plots (right) at junction temperatures of 40C and 80C.

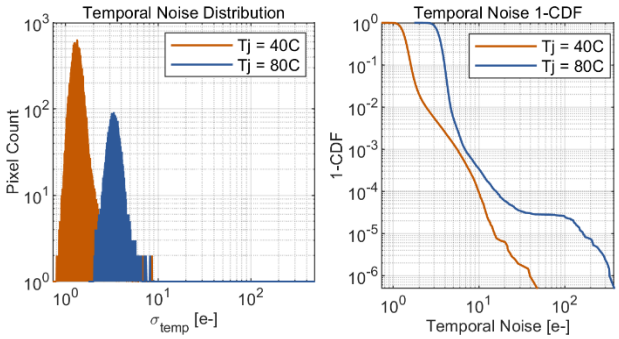

Figure 7. Dark temporal noise variance histograms (left) and 1-CDF plots (right) at 40C and 80C.

Photon-Transfer and SNR Curves

Figure 8 presents a photo of the setup that was used for the measurement. It included a demo camera with a 1 MP automotive image sensor and a 36-patch 150 dB Imatest test chart with a DarkWorld mask that was placed on an LED light panel. An

example with a 36-patch 134 dB Image Engineering test chart is shown in the IEEE P2020 Noise standard [4].

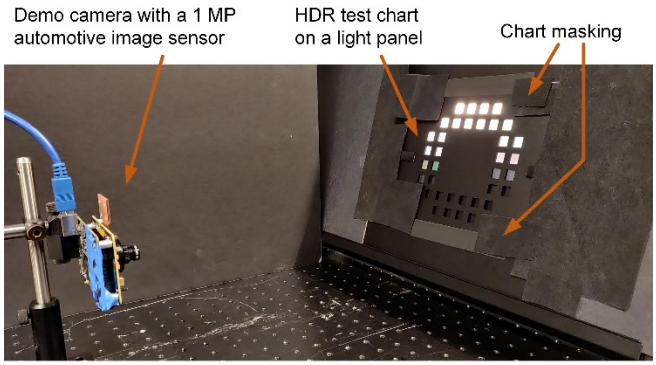

Figure 8. An automotive camera is positioned in front of an HDR test chart that is placed on an LED light panel in the setup that was used to collect data to construct the photon-transfer and SNR curves of the camera.

There are challenges to this measurement. Glare, which is caused by internal reflections inside the camera module, increases signal value of all pixels. Lens reflections produce an image of the brightest patches of the chart in the image region of the darkest patches if the camera is aligned to have the center of the chart roughly located at the center of the pixel array, as shown in Figure 9. Lastly, the user should ensure that there are no reflections of the camera in the chart.

These challenges are manageable, and it is possible to extract useful sensor-level noise IQFs from image sets of HDR test charts. To minimize glare, all chart areas, excluding the patches, should be covered by material that is opaque and matte for the relevant spectrum. With the chart that was used here, registration marks at the four corners of the chart were covered, as shown in Figure 8.

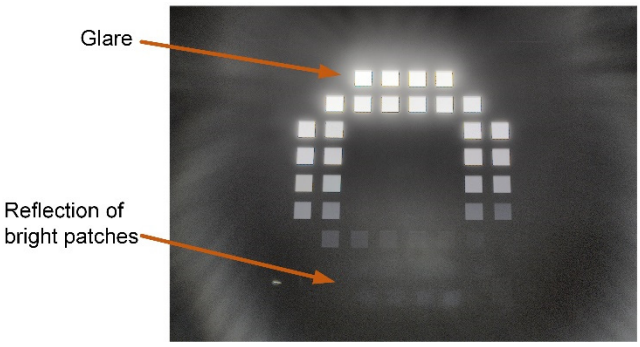

Figure 9. Challenges with HDR test charts. Glare is a result of internal reflections inside the camera module. Lens reflections of the brightest patches appear in the image region of the darkest patches, making them unusable.

Image sets may need to be captured with more than one light level due to glare. Figure 10 presents two images from two image sets that were captured for this work, one when the power of the LED panel was set to 100% and one when it was set to 0.4%. When the power of the LED panel is 100%, as shown in the top image, the most transparent patch is saturated, as needed in order to obtain saturation level. However, although the dynamic range (DR) of the sensor with the 3-exposure configuration file that was used for the measurement was lower than the dynamic range of the chart, it was not possible to cover the entire DR of the sensor with this light level because, due to glare, signal level of the least transparent patches was higher than the dark level of the image sensor. The image set that was captured with 0.4% LED power allowed to cover the low signal range down to dark.

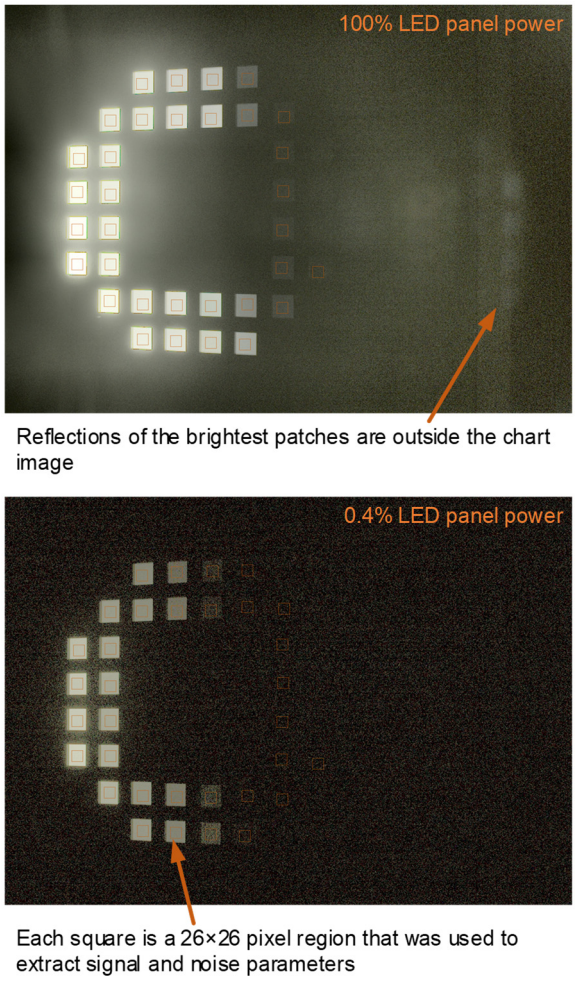

Figure 10. Images from the 100% and 0.4% LED power image sets. Both were needed to cover the sensor DR because of glare. The camera was rotated by 90° and aligned to have the center of the chart image at some distance away from the center of the pixel array to get the reflections of the brightest patches of the chart outside the chart image.

Lens reflections of the brightest patches are unavoidable. But to prevent their appearance in the area of the chart image, the camera was rotated by 90° and aligned to obtain the center of the chart image at some distance away from the center of the pixel array. Each square represents a 26×26 pixel-region that was used for analysis. Uniformity was evaluated manually in each selected pixel-region. Some of the least transmissive patches had to be excluded because their signal level was very similar.

Signal and noise parameters were calculated for each region, and results were used to construct PTC and SNR curves, as shown in Figure 11.

To calculate system gain, SG, one must first find a shot-noise limited region in the SNR_{temp} curve. Shot-noise follows Poisson statistics, therefore, in a shot-noise limited region: $\sigma^2_{e-} = S_{e-}$, where S_{e-} and σ_{e-} are signal and noise in charge units, respectively. Conversion to signal and noise in DN, S_{DN} and σ_{DN}, respectively, gives the following relationship: $\sigma^2_{DN} = SG \cdot S_{DN}$. SNR_{temp} in this region is approximately $20 \cdot \log_{10}(\text{sqrt}(S_{DN}/SG))$, and this results in a 10 dB/dec slope. Small deviations from this value are expected because of typical process variations. However, large deviations indicate that shot noise is not the dominant noise, which can be a result of noise that is added by a circuit at the periphery [7]. In these situations, it is not possible to calculate a reliable SG value.

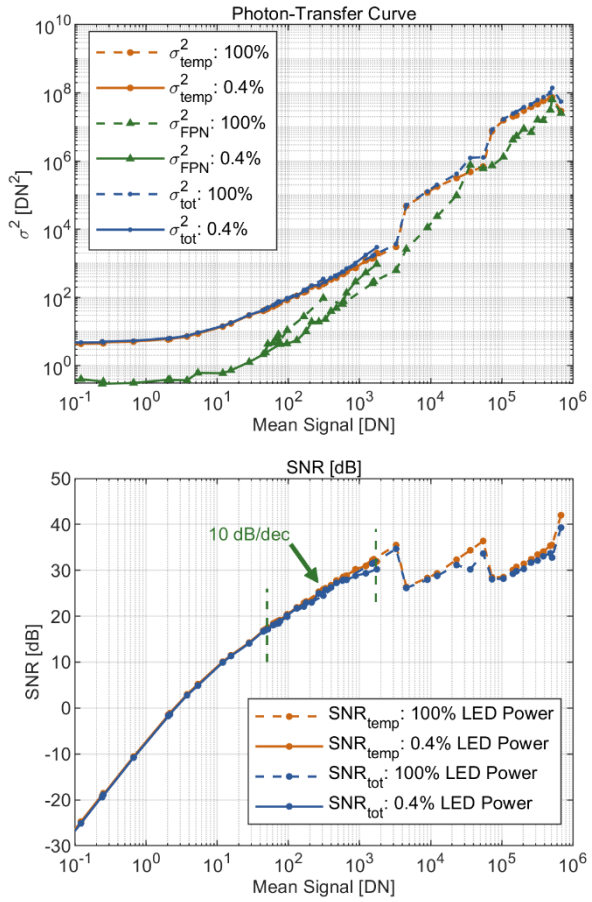

Figure 11. PTC and SNR curves of the automotive camera with the 1 MP sensor that was activated in 3-exposure HDR mode, as constructed using data from the two image sets in Figure 10. The arrow in the SNR plot points to the signal region where the slope of the SNR_{temp} curve is 10 dB/dec.

With the camera that was used in this work, a shot-noise limited region was identified in mean signal values between 50 and 1,700 DN, as shown in the top plot of Figure 12. The same signal range was then used to calculate SG from the PTC curve, as shown in the next plot of the same figure, and results gave that SG = 0.92 DN/e-. SNR1 was extracted from the SNR_{tot} curve by interpolation of data points that were just above and just below 0 dB, as shown in the third plot. S_{EFW} and S_{sat} were obtained from the photon-transfer curve, as shown in the bottom plot of Figure 12. All numbers in DN and charge units are summarized in the Table I.

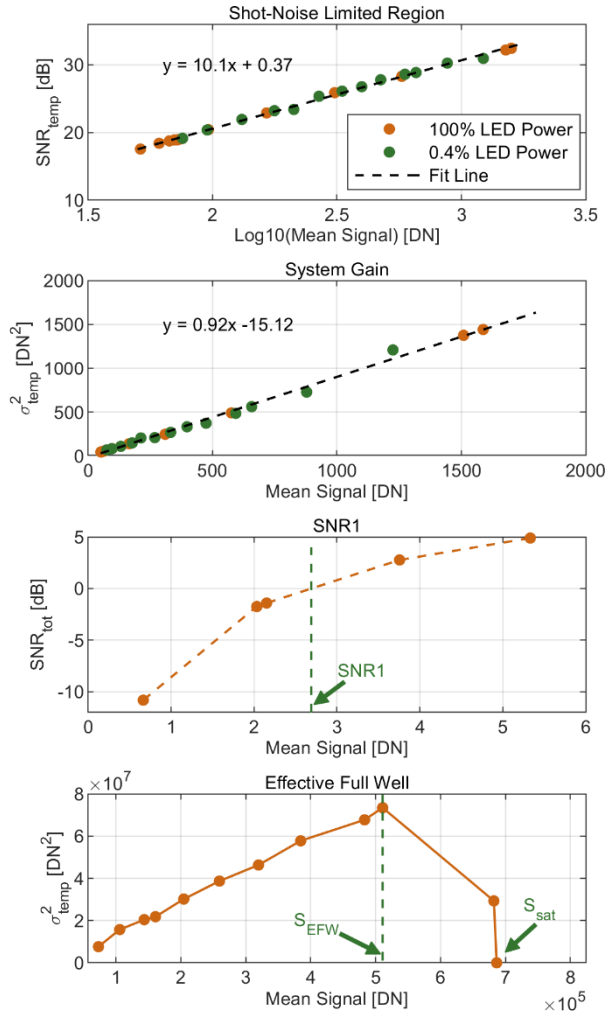

Figure 12. Extraction of noise IQFs from the curves in Figure 11.

Table I. Summary of Noise IQFs from PTC and SNR Curves

IQF	Value
SG	0.92 DN/e-
SNR1	2.69 DN = 2.86 e-
S_{EFW}	510,764 DN = 555 ke-
S_{sat}	686,424 DN = 746 ke-

Signal Falloff

Figure 13 presents the setup that was used to capture images for the signal falloff test. A diffuser is placed in front of a camera that is pointed at a light panel. Noise filtering and removal of local high frequency fluctuations due to temporal noise and FPN is important for signal falloff measurements as the goal is to describe the general shape of the curve. There are challenges in fitting a curve. First, the model form can be wrong. With correct model forms, an order that is too low has the benefit of lower computational power, but also low accuracy. An order that is too high may fit the noise in a specific camera, but not general enough to be used with all cameras from the same series.

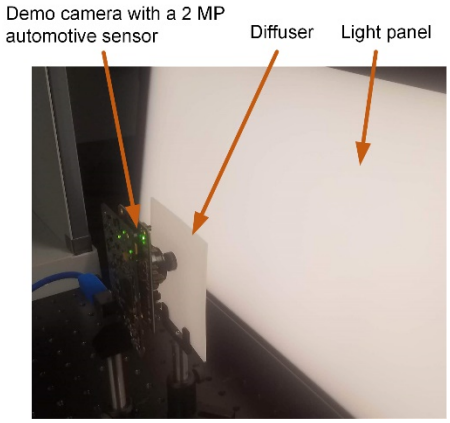

Figure 13. The setup to capture signal falloff images. A diffuser is placed in front of a demo camera that is pointed at a light panel.

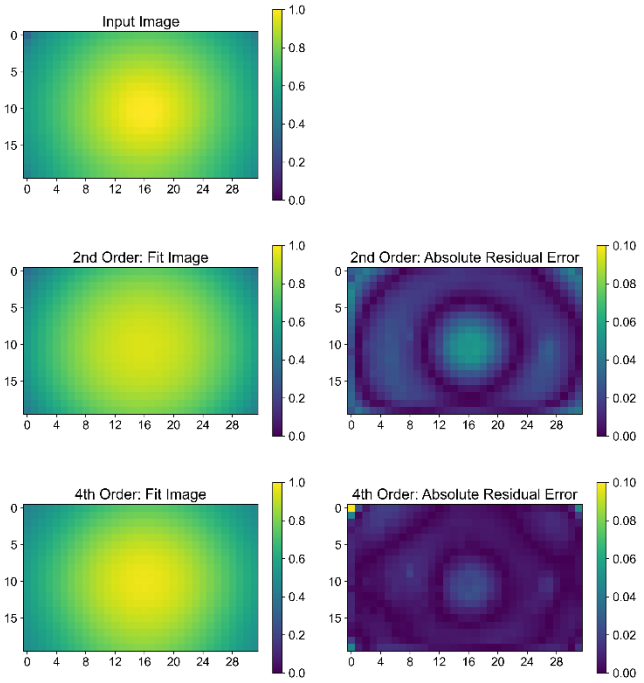

Figure 14. Signal falloff results with 2nd order and 4th order polynomial fit.

Figure 14 presents an input image, images that were produced from 2nd order and 4th order polynomial fits, and corresponding absolute error images. The original image is the camera #1 signal falloff image of the Gr channel from Figure 5, where temporal noise filtering was applied by image averaging. Spatial noise is filtered by dividing the image into 20×32 blocks of 16×16 pixels per color channel to produce the input image in Figure 14.

One may observe that signal falloff from the center to the edge of the image is sharper in the input image than in the two fit images. The absolute residual error images confirm that the error in the center is high. Those images also show high error around columns 25-26 and rows 9-11. This may indicate that there was some contamination on the lens or on the package of the sensor during image capture. Lastly, with the 4th order fit, the absolute residual error is rather high at the corners. This may be acceptable depending on the useful image height for the end-user application. If, for example, the application only uses 80% image height, high error at the corners would not impact performance.

Conclusion

The IEEE P2020 Noise standard addresses operating modes and conditions that are relevant to automotive cameras. This work presented sensor-level noise IQFs that were extracted from dark statistics at 40C and 80C, and from photon-transfer and SNR curves that were constructed for an automotive camera that was activated in 3-exposure HDR mode and tested with a HDR target. This work also presented camera-level noise IQFs for the signal falloff metric from work that was done with an automotive camera.

Acknowledgement

The authors thank all IEEE P2020 Working Group participants who reviewed the standard drafts and provided constructive feedback, mainly, Uwe Artmann, Rob Sumner, and Hans Li. The authors also thank Rujul Desai, Shaheen Amanullah, and Radu Ispasoiu for feedback and data.

References

[1] European Machine Vision Association, "EMVA Standard 1288 - Standard for Characterization of Image Sensors and Cameras, Release 4.0 Linear," 2021.

[2] *ISO 15739:2013 Photography — Electronic still-picture imaging — Noise measurements,* 2013.

[3] IEEE-SA P2020, "IEEE P2020 Automotive Imaging," IEEE, 2018.

[4] IEEE P2020 Automotive Image Quality Working Group, *Noise standard draft Rev. 8,* 2022.

[5] J. R. Janesick, Photon Transfer DN to Lambda, SPIE Press, 2007.

[6] A. Darmont, High Dynamic Range Imaging, 2nd ed., Bellingham, WA: SPIE, 2019.

[7] S.-F. Yeh, M.-H. Wu, C.-L. Lee, C. Yin, K.-Y. Chou, H.-Y. Tu and C. Y.-P. Chao, "Impact of Kickback Noise of Comparator in Single Slope ADC on Photon Transfer Curve Characterization," in *International Image Sensor Workshop*, 2021.

Author Biography

Orit Skorka received her BSc from Ben-Gurion University of the Negev, Israel, in 2001, her MSc from the Technion IIT, Israel, in 2004, and her Ph.D. from the University of Alberta, Canada, in 2011, all in Electrical and Computer Engineering. She joined Aptina in 2013 and is now with the Intelligent Sensing Group at onsemi working on pixel characterization and image quality of CMOS image sensors for automotive, security and other imaging applications.

Paul Romanczyk received both his B.S. and Ph.D. in Imaging Science from Rochester Institute of Technology (2009, 2015). He is currently a Senior Imaging Scientist at Imatest, LLC., where he develops tests and metrics for assessing image quality and camera performance.